Received 15 January 2024; revised 1 March 2024; accepted 9 March 2024. Date of publication 14 March 2024; date of current version 27 May 2024.

Digital Object Identifier 10.1109/OJAP.2024.3377264

Intelligent Signal Coverage Employing Hybrid-Mode Excitation in 5G Spoof Surface Plasmon Polaritons Antennas

BEHNAM MAZDOURI AND RASHID MIRZAVAND (Senior Member, IEEE)

Department of Electrical and Computer Engineering, University of Alberta, Edmonton, AB T6G 1H9, Canada

CORRESPONDING AUTHOR: B. MAZDOURI (e-mail: mazdouri@ualberta.ca)

This work was supported in part by NSERC; in part by Alberta Innovates; in part by TELUS Inc.; and in part by CMC Microsystems.

ABSTRACT Multi-directional signal coverage utilizing simple multi-functional antenna plays a crucial role in 5G smart environment and the massive Internet of Things (IoT). The term "Multifunctionality" refers to an antenna's ability to control and alter its radiation pattern. Spoof Surface Plasmon Polariton (SPP) antennas are considered simple and cost-effective due to their flexible one-layer configurations, making them a good candidate for smart environment. Different radiation features and signal levels in the spoof SPP antenna employing either separated or combined k_{-1} space harmonic or odd-mode are considered in this paper. Our proposed hybrid-mode antenna combines the above mentioned modes. For this purpose, a phase shift stub (PSS) is proposed for providing required phase delay. Then, the PSS is connected to a sinusoidally impedance-modulated spoof SPP antenna for hybrid-mode excitation. Our antenna supports radiation features of the mentioned modes in separate and hybrid-modes, depending on phase delay value of PSS at the operating frequencies of 26 GHz-30 GHz. Furthermore, a new design guide for odd-mode spoof SPP antennas is introduced in order to decrease side lobes' level that are more intense in longer antennas. In order to verify the proposed structures' performance, simulated and measured results of the reconfigurable antenna consisting of diodes and a biasing circuit are presented. The obtained measured results align well with the simulated ones.

INDEX TERMS Intelligent coverage, even- and odd-modes, surface wave, surface plasmon antenna, hybrid-mode.

I. INTRODUCTION

With the rapid development of wireless communication systems, the concept of smart environment has been introduced to intelligently control signal coverage, connect massive number of users and machines for data transmission, and improve energy efficiency of the systems [1]. The high data rate and low latency of new generation of telecommunication network, i.e., 5G, pave the way for intelligent Machine to Machine (M2M) or Device to Device (D2D) connectivity, known as Internet of Things or IoT [2]. Modern communication systems require reconfigurable components, such as reconfigurable transmitters and receivers comprised of antennas, for multifunctional data transmission. Instead of employing multiple antennas in order to provide different radiation features, one antenna can be designed with capability of reconfiguring its structure to transmit data in desired directions. Therefore, utilizing fewer antennas leads to a reduction in volume, weight, and costs of system implementation.

In addition to reducing number of antennas, the simplicity of the antenna's configuration is of great importance. A one-layer spoof SPP antenna, including a corrugated metal, can be a good candidate. In fact, at microwave frequencies, the corrugated metal is created by connecting periodic unit cells in order to mimic behavior of highly localized surface waves that naturally propagate in interference of metal and dielectric at optical frequencies [3], [4]. Spoof SPP-based structures are widely used in microwave applications such as filters [5], [6], [7], [8], odd-mode antennas [9], [10], [11], [12], [13], and leaky wave antennas (LWAs) [14], [15], [16].

For odd-mode radiation, a pattern reconfigurable antenna for wide angle beam steering was designed by controlling the status of three PIN diodes [9]. The antenna supports even- and odd-modes current distributions separately for radiating

at the broadside or the endfire directions, respectively [9]. A high aperture efficiency endfire antenna based on a pair of spoof SPP TLs supported by a balun with a 180° phase shifter has been reported in [10]. Each pair of the spoof SPP units works as a dipole. The antenna operates in the frequency range of 9–11 GHz with an average gain of 11.51 dBi. In that structure, the feeding part requires a ground plane in bottom layer that makes the structure two layers instead of one layer. An endfire antenna with accumulation and subtraction beams was designed based on phase transforming of spoof SPP structure [11]. The antenna includes asymmetric double-sided corrugation to provide asymmetric electromagnetic field [11]. In [12], a shared aperture antenna based on odd- and even-modes excitation has been introduced to give broadside, tilted, and endfire radiation performances. A fish-bone shaped endfire antenna fed by a microstrip to slot line converter and a differential-mode exciter has been introduced in [13]. Similar researches in [17], [18], [19], [20], [21] have been reported concerning the odd-mode spoof SPP antennas.

To the best of authors' knowledge, the previous researches have presented different approaches for the spoof SPP antenna by exciting one mode or two modes separately. Novel odd- and hybrid-modes spoof SPP antennas consisting of a phase shift stub (PSS) are proposed with the purpose of simultaneously achieving radiation features of both modes. Furthermore, a new design guide for decreasing side lobes' level in the odd-mode antenna is presented according to number of antenna's cells and the cells' dispersion diagram. Fig. 1 illustrates potential application of our proposed reconfigurable hybrid-mode antenna communicating with the targets in the space (Sat 2 to 5) and on the earth (Base station 1 to 3). Satellite 1 (Sat 1) simultaneously transmits signals to the targets at different angles (θ_1 and θ_2) and shorter or longer distances at a fixed angle of θ_1 (r_3 and r_4). Our proposed reconfigurable hybrid-mode antenna provides beam scanning by varying frequency from k_{-1} space harmonic, for example from θ_1 to θ_2. Additionally, the antenna transmits or receives signals in its endfire direction (Base station 1) while communicating with sats or base stations in other locations. The hybrid-mode radiation feature comes in useful for a satellite communicating at the same time with a fixed base station on the earth (Base station 1) and targets in different locations. Moreover, the antenna is capable of controlling its signal coverage level intelligently based on devoting different shares of its radiated power to k_{-1} and odd-modes. Intelligent controlling radiation of the two mentioned modes is done by designing and fabricating an active PSS including three PIN diodes and a biasing circuit.

This paper is structured as follows, Section II describes our proposed novel PSS for odd-mode excitation in the spoof SPP antennas. Also, a new design guide for designing odd-mode antennas with enhanced side lobes' level is presented. Hybrid-mode excitation is introduced in Section III. Simulated odd, k_{-1}, and hybrid-modes antennas are compared in this section. Furthermore, simulated and fabricated reconfigurable hybrid-mode antenna are discussed for the purpose of intelligent signal coverage. Finally, conclusions are drawn in Section IV.

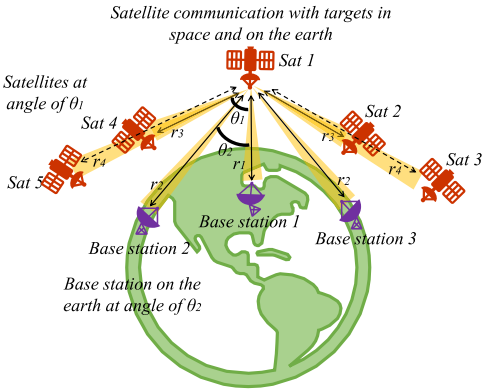

FIGURE 1. Potential application of the proposed reconfigurable hybrid-mode antenna.

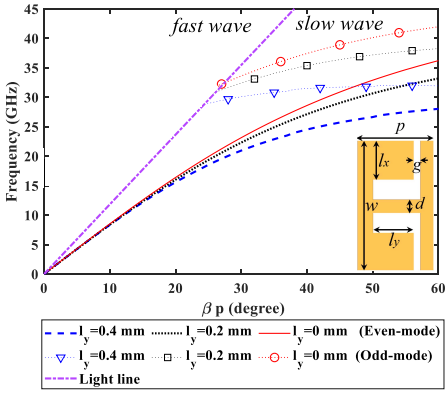

FIGURE 2. Even- and odd-modes dispersion curves of double-sided L-shaped unitcell with p=0.7, w=2.34, g=0.07, and d=0.2 (all in mm).

II. ODD-MODE EXCITATION IN SPOOF SPP ANTENNA

In this section, our proposed method for odd-mode excitation in the spoof SPP structures is introduced. Fig. 2 shows the dispersion diagram and the unit cell's design, including the double-sided L-shaped grooves. Dimensions of the cell which are period of p, the gap between grooves g, width and length of the L-shaped part l_x and l_y, width of cell w, and width of central conductor d determine its dispersion curve. Dispersion diagrams of the cell with different values of l_y in even- and odd-modes were computed using Eigen mode simulations in CST. In Eigen mode simulations, periodic and perfect electric conductor (PEC) boundary conditions were used to obtain dispersion curves. It is evident that the curves for even-modes are non-radiative since they are located in the slow-wave region. The non-radiative part of odd-mode dispersion graphs corresponds to larger values of cell's phase constant than that of light. For simple case of corrugated conducting surface (I-shaped cells extended to infinity from bottom side), there is a theoretical analysis with

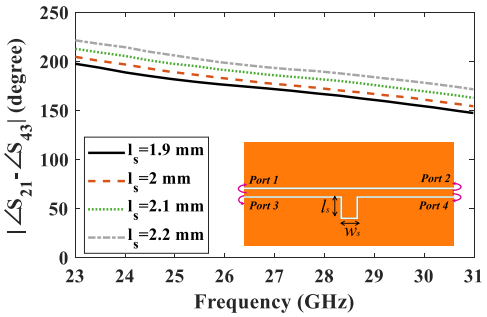

FIGURE 3. Phase shift versus frequency of the proposed PSS for different values of l_s from 26 to 30 GHz.

assumption of each corrugations as a short-circuited parallel plates leading to the following eigen value equation [22]:

$$\frac{d}{p}\sum_{n=-\infty}^{\infty}\frac{1}{\tau_n h\tan(\tau_n b)}\left(sinc\left(\frac{\beta_n d}{2}\right)\right)^2=\frac{1}{kh\tan(kh)} \quad (1)$$

where p is period of the unitcell, and the rest of geometrical parameters were defined according to cell's configuration introduced in [22].

According to formula (1) and dispersion results reported in [22], the odd-mode dispersion diagram does not start at zero and it is located in the fast-wave region. Therefore, this mode has necessary condition for radiation at lower frequencies in the mentioned region. In our design, a closed-form equation for dispersion graphs cannot simply be obtained due to more complex configuration of the cell (or any other unit cells in the literature with different shapes) on the substrate. But dispersion curves indicates similar behavior to that of introduced cell in [22]. To excite odd-mode, the proposed PSS is connected to the CPW for phase shift provision according to Fig. 3, and length of l_s tunes amount of phase delay. To evaluate the PSS's performance, four lumped ports were defined in the two gaps of the CPW. Fig. 3 depicts phase difference between port 2 and 4, ie S_{21} and S_{43}, at frequencies from 26 to 30 GHz. For l_s=1.9 mm, 180° ± 10° phase difference is obtained. Fig. 4(a) depicts our proposed odd-mode antenna including the PSS and L-shaped unit cells with p=0.7 mm and w=2.34 mm. The PSS's location has effect on both input impedance and mode change from confined even mode to the radiative odd-mode. Therefore, adding the PSS is more complex than adding a simple stub to the circuit. So, its location can be optimized using full-wave simulations. The length of l_y was varied from 0.3 mm to 1.9 mm to consider its effect on matching of the antenna to the air. According to Fig. 4(b), in our design, closer PSS to the mode converter (or smaller l_y) results in better matching. Fig. 4 (c) displays the radiated electric field from the proposed odd-mode antenna. The odd-mode endfire antenna is radiative thanks to satisfying necessary conditions of its fast-wave dispersion diagram and its open boundary condition at the angle of radiation or at the endfire direction.

As mentioned in [13], in odd-mode, the spoof SPP cells can be modeled as an array of dipoles. The similarity of the

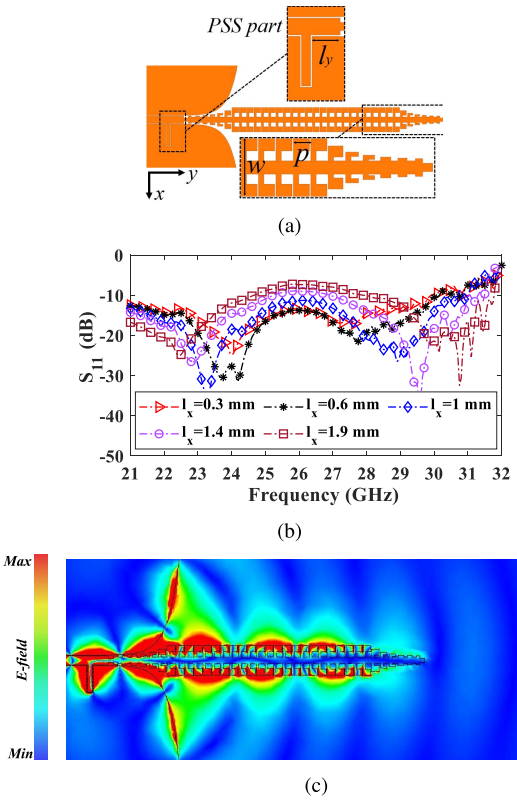

FIGURE 4. Proposed odd-mode spoof SPP antenna. (a) Antenna's configuration. (b) Tuning scattering parameter S_{11} by varying the PSS's distance to the transition circuit l_x. (c) Radiated electric field on the proposed antenna.

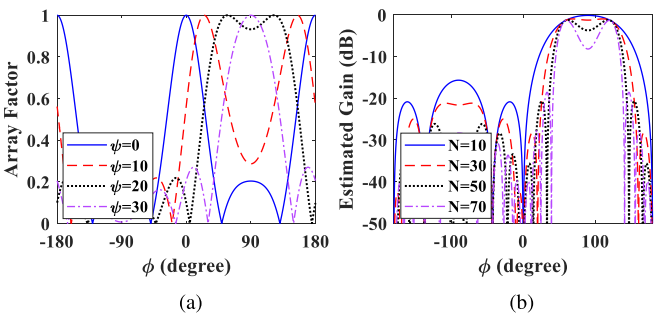

FIGURE 5. Radiation pattern estimation of odd-mode spoof SPP antenna. (a) Array factor of N=50 cells for different values of ψ= 0, 10, 20, and 30 degrees in θ=90 degree plane. (b) Calculated gain of the antenna consisting of N=10, 30, 50, and 70 cells in θ=90 degree plane.

current distribution on the cells and the dipole antenna is the reason for this assumption. This method merely gives an approximation of radiation pattern in the spoof SPP antennas. Each cell is modeled as a point source with phase of ψ determined by its dispersion diagram. Fig. 5(a) and (b) demonstrate the AF for N=50 cells and gain of the whole array in a constant phase of ψ= 20°, respectively. From Fig. 5, it can be concluded that the longer spoof SPP antenna or larger value of N causes ripples (side lobes) in the antenna's gain graph. This is an important point in designing an odd-mode spoof SPP antenna.The dipole assumption approximates the radiation pattern; hence, full

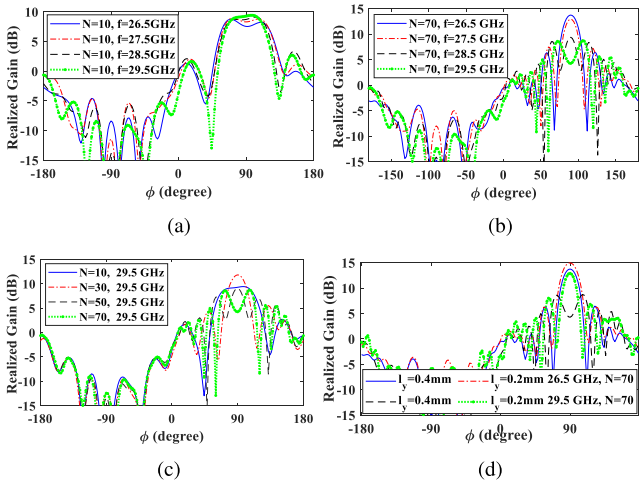

FIGURE 6. Consideration of ripples' creation in the odd-mode antenna's radiation patterns. Gain at different frequencies of (a) short antenna (N=10) and (b) long antenna (N = 70). (c) N effect on the antenna's gain by varying from 10 to 70 at 29.5 GHz. (d) Comparison of gain enhancement of long antenna by reducing l_y from 0.4 mm to 0.2 mm.

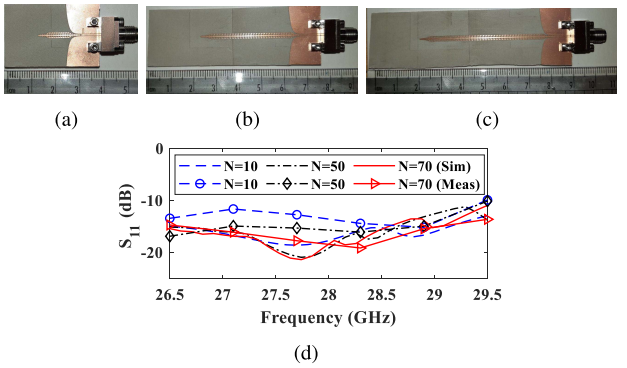

FIGURE 7. Fabricated odd-mode spoof SPP antennas including a) N=10 cells (2.5 cm*3.9 cm) b) N=50 cells (2.5 cm*7.7 cm) c) N=70 cells (2.5 cm*9.3 cm). d) Simulated and measured S_{11} of the antennas.

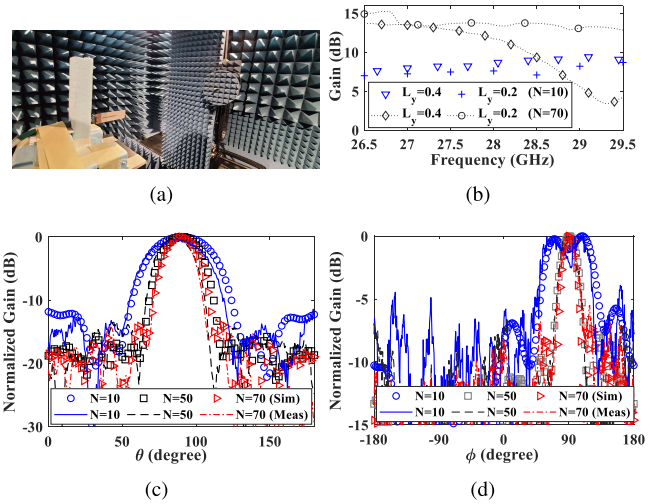

FIGURE 8. Radiation pattern measurement of the introduced antennas. (a) Experimental setup with antenna under test (AUT). (b) Simulated gain versus frequency of the antennas. (c) Simulated radiation pattern of the antennas in comparison with the measured ones at 28 GHz (d) in ϕ=90° and (c) θ=90°.

wave simulations were done in order to verify this effect. Fig. 6 demonstrates the effects of N and cut-off frequency of f_c on the radiation pattern of the proposed antenna. The cut-off frequency of the L-shaped cell is 32 GHz in order to be radiative from 26.5 GHz to 29.5 GHz according to the dispersion curves in Fig. 2. For the purpose of considering N effect, the antenna consisted of 10 cells. The radiation patterns in Fig. 6(a) at the frequencies of 26.5, 27.5, 28.5, and 29.5 GHz indicate approximately a flat gain from ϕ=70 to 110 degrees in the endfire direction. To achieve high directivity, N was increased from 10 to 70 cells. As depicted in Fig. 6(b) for N=70, the radiation patterns are more directive at lower frequencies like 26.5 GHz compare to that of higher frequencies like 29.5 GHz with side lobes approximately equal to the main lobe. This problem results in lower gain at higher frequencies. To have a better insight into this effect on the radiation performance, radiation patterns for different values of N at the frequency of 29.5 GHz were presented in Fig. 6(c). According to this figure, by increasing N from 10 to 30, the antenna 's gain is increased but further increase of N from 30 to 70 leads to creation of ripples in the radiation pattern or existence of the side lobes. Fig. 6(d) illustrates effect of f_c on the antenna's gain for $N = 70$. It can be concluded that lower f_c results in higher gain. Therefore, the parameters of N and f_c can be optimized in order to increase directivity and gain of the odd-mode antenna.

To verify the obtained simulated results, three antennas made of N= 10, 50, and 70 cells with period of p= 0.705 mm were fabricated on RO4003c with thickness of 0.3 mm. Fig. 7(a) to (c) demonstrate the fabricated antennas. Simulations and measurements agree well on the scattering parameter S_{11} as can be seen in Fig. 7(d). Fig. 8(a) shows our experimental setup in an anechoic chamber. Fig. 8(b) depicts simulated gain improvement of the proposed odd-mode antenna versus frequency by choosing higher cut-off frequency of f_c. The waveguide probe WR-28 was used as the antenna transmitter. In Fig. 8(c) and (d), the normalized radiation patterns were shown for $\phi = 90°$ and $\theta = 90°$ planes, respectively. The antennas were tested at the frequency of 28 GHz and no large ripples were observed in the radiation pattern that proves veracity of the suggested design guide. For the small antenna the parameter l_y is 0.4 mm while 0.2 mm is selected for the longer antennas to have a lower phase difference at each unit cell. The measured antennas' gain, at 28 GHz are 8.5 dB, 12.2 dB, and 13.8 dB for N= 10, 50, and 70, respectively. Since we have TM surface waves along the antenna in y-axis, the main polarization in odd-mode is parallel to x-axis and cross-polar is parallel to z-axis. The calculated cross-polarization from HFSS simulation is better than −20 dB at the frequency of 28 GHz.

III. HYBRID-MODE EXCITATION IN SPOOF SPP ANTENNAS

Hybrid-mode spoof SPP antenna operates based on the simultaneous excitation of either k_{-1} space harmonic or odd-modes in a sinusoidal impedance-modulated antenna.

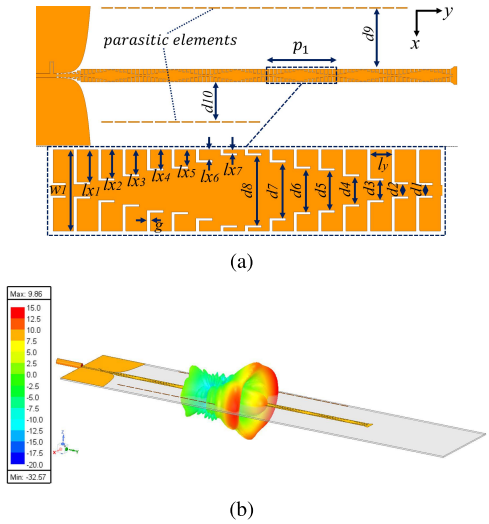

FIGURE 9. Spoof SPP antenna including six impedance modulated blocks. The geometrical parameters are: w_1=2.4, p_1=10.69, l_{x1}=0.93, l_{x2}=0.82, l_{x3}=0.7, l_{x4}=0.53, l_{x5}=0.48, l_{x6}=0.3, l_{x7}=0.1, l_y=0.61, g=0.11, d_1=0.3, d_2=0.34, d_3=0.56, d_4=0.8, d_5=1.15, d_6=1.24, d_7=1.6, d_8=2, d_9=10, d_10=6 (all in mm). (b) 3D radiation pattern on the antenna's structure at the frequency of 28 GHz.

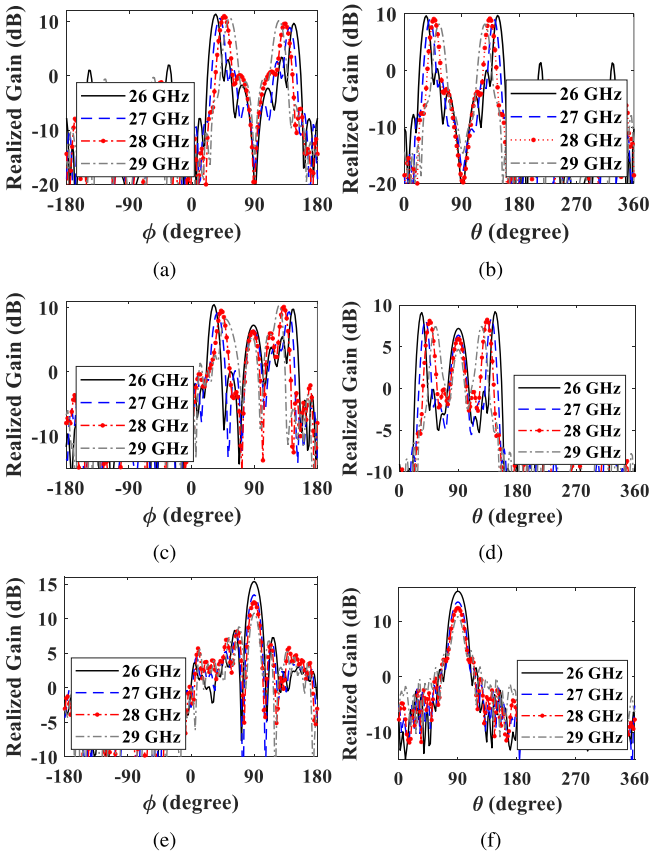

FIGURE 10. Simulated radiation patterns of the (a) k_{-1} mode $\theta = 90^\circ$ plane (b) k_{-1} mode $\phi = 90^\circ$ plane (c) hybrid-mode $\theta = 90^\circ$ plane (d) hybrid-mode $\phi = 90^\circ$ plane (e) odd-mode $\theta = 90^\circ$ plane (f) odd-mode $\phi = 90^\circ$ plane.

The design procedure for the impedance modulated spoof SPP antenna has been well discussed in [23]. Fig. 9(a) shows our designed impedance-modulated spoof SPP antenna, including six modulated blocks. Since the power leaks by travelling along the antenna, the antenna's length should be long enough to achieve optimal energy leakage. The period of unit cells p and modulation period p_1 are 0.705 mm and 10.69 mm, respectively. The rest of geometrical parameters were provided in the caption of this figure. Since the hybrid-mode antenna encompass odd-modes, design considerations of the both modes should be optimally satisfied. Additionally, the current distribution of hybrid mode is combination of symmetric k_{-1} and asymmetric odd modes, resulting in asymmetric radiation pattern of k_{-1} mode. Hence, two asymmetric parasitic components, shown in Fig. 9(a), have been added on the top and bottom sides of the antenna as a compensation. Depending on the distance and length from the antenna, parasitic elements can affect the radiated field. Electromagnetic energy is coupled to these elements at different distances, resulting in manipulation of radiated power. The optimal size and location of the elements were determined according to full-wave simulations in HFSS. To have a general view about radiation of the hybrid-mode antenna, 3D radiation pattern with the structure of the antenna in the hybrid-mode at the frequency of 28 GHz was provided in Fig. 9(b). According to ref [23], the calculated leaky wave antenna's parameters are effective surface refractive n=1.81, modulation factor M=0.63, maximum and minimum of surface impedance 920.85 and 206.51 corresponding to the designed unit cells' dimensions. Based on the mentioned parameters, radiation angle of the leaky wave antenna is 35°. The radiation angle in the simulations and measurements are very close to 35°. Fig. 10 demonstrates simulated radiation patterns of the antenna for the k_{-1} ($l_s = 0mm$), hybrid ($l_s = 0.8mm$), and odd ($l_s = 2mm$) modes at the frequencies of 26, 27, 28, and 29 (all in GHz). From Fig. 10(c) and (d), it can be concluded that radiation patterns of the hybrid-mode is combination of the k_{-1} and odd-modes illustrated in Fig. 10. In Fig. 11, simulated electric field distribution of the k_{-1}, hybrid, and odd-modes at the frequency of 28 GHz were given to intuitively show the difference among the three modes.

According to the simulated results in Fig. 10, the amount of phase delay provided by the PSS controls radiation shares of k_{-1} and odd-modes. The antenna changes its radiation performance only by varying the PSS's length as a small part. Consequently, our proposed antenna can be a good candidate as a reconfigurable antenna requiring minimum number of controlling elements. As an example, PIN diodes can be employed for varying the PSS length. Fig. 12 demonstrates the schematic of an active PSS including three PIN diodes and a biasing circuit for hybrid- and odd-modes radiations in one antenna's configuration. In the circuit, two voltages of V_1 and V_2 are applied to the circuit with common ground planes. For odd mode excitation, D_1 is in ON state while D_2 and D_3 are in OFF state. Hence, positive voltage of V_2 and negative voltage of V_1 are required.

TABLE 1. Comparison with other spoof SPP antennas.

Ref	f_0 (GHz)	size (L(λ_0) *W(λ_0))	Maximum odd Gain (dB)	Maximum K_{-1} Gain (dB)	Band width (GHz)	Radiation efficiency (%)
[23]	9.3	1.4*16.9	———	13.5	8.8 - 9.3	95
[9]	5	3.7*0.8	9	7.2	4.85 - 5.25	———
[10]	10	1.7*0.51	12.2	———	9 - 11	98
[11]	5.5	3.91*0.66	10	———	less than 0.5	———
[12]	14	1.5*1	6.78	———	11 - 17.38	75
[13]	3.7	1.36*0.86	8.6	———	2.4 - 5	90
[17]	6	2.33*0.25	7.9	———	4.9 - 7	54
[18]	40	7.6*2.45	15	———	25 - 52	95
This work odd-mode	28	9*1.8	15.2	———	26.5 - 29.5	81
This work hybrid-mode	28	12*2.5	6.8	9.33	26.5 - 29.5	75

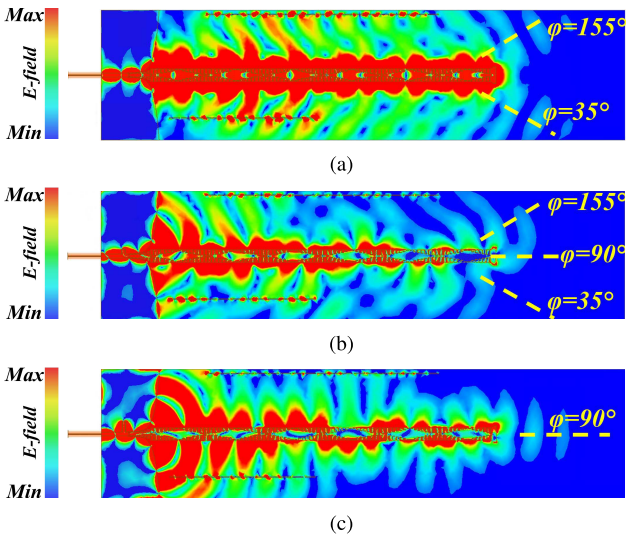

FIGURE 11. Simulated electric filed distribution on the antennas' structure in (a) k_{-1} mode (b) hybrid-mode and (c) odd-mode antenna.

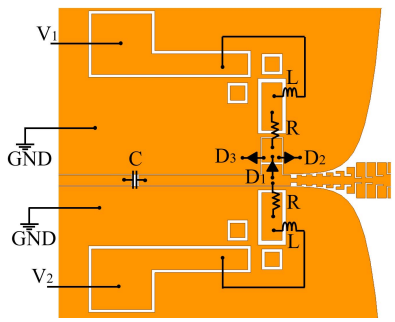

FIGURE 12. Proposed biasing circuit for the three diodes for hybrid and odd-modes excitations.

Values of voltage can be controlled out of the designed bias circuit. For the hybrid-mode scenario, D_2 and D_3 are in ON state and D_1 is OFF. Therefore, V_1 and V_2 are positive and negative, respectively. Fig. 13(a) presents the fabricated reconfigurable antenna consisting of the active PSS for the odd and hybrid-modes excitations. Three diodes (MADP-000907-14020P), two inductors (BCR-122JLB), one

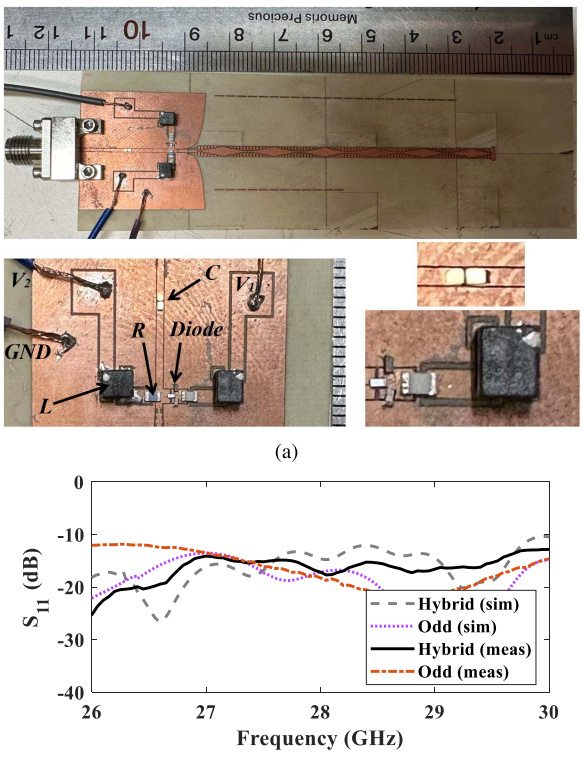

FIGURE 13. Fabricated reconfigurable spoof SPP antenna. (a) the antenna including biasing circuit and zoom-in pictures of the lumped components. (b) Simulated and measured scattering parameter of S_{11} in the hybrid and odd-modes.

capacitor (P62BNL820M5S), and two resistors (CH0603-100RJNT) were used for the active PSS. The width of PSS (w_s) can be designed wide enough in order to have more space for soldering the diodes. Fig. 13(b) shows simulated and measured S_{11} parameter of the antenna in the both mentioned modes. Moreover, normalized radiation patterns of the reconfigurable antenna from simulation and measurements at the frequency of 28 GHz were compared in Fig. 14. Good agreements between the measured and simulated results was found. Table 1 compares performance of the hybrid- and odd-modes antennas to the antennas presented in the literature.

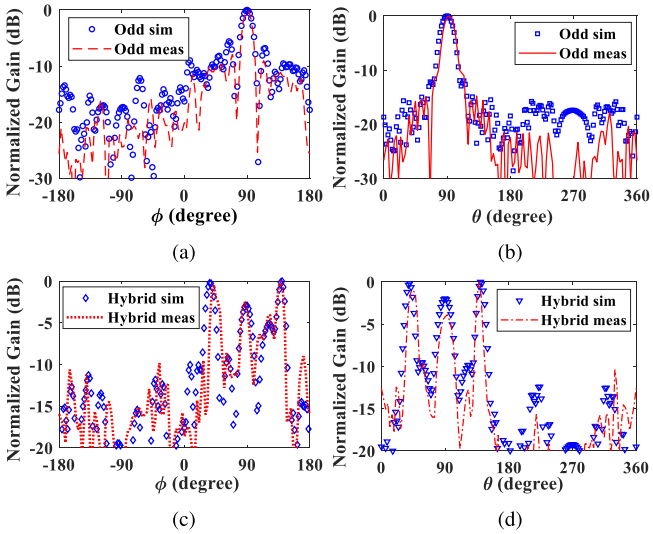

FIGURE 14. Simulated and measured radiation patterns of the reconfigurable antenna in (a) odd-mode $\theta = 90°$ plane (b) odd-mode $\phi = 90°$ plane (c) hybrid-mode $\theta = 90°$ plane (d) hybrid-mode $\phi = 90°$ plane.

IV. CONCLUSION

A novel method for odd-mode excitation in the spoof SPP antennas was introduced in this paper. The proposed method is based on one-layer phase shift stub, or PSS, that was simply integrated to a CPW line. The PSS provides 180° phase delay in order to stimulate the odd-mode radiating in the endfire direction. Our theoretical and simulated results indicate ripple appearance for longer antennas, especially at higher frequencies. Hence, two parameters of number and cut-off frequency of cells (N and f_c) were considered in order to decrease side lobes' levels.

In addition to odd-mode stimulation, the PSS is capable of exciting hybrid-mode by providing a phase delay between 0° to 180°. The new hybrid-mode spoof SPP LWA combines radiation features of k_{-1} and odd-modes in one antenna body. In fact, the antenna radiates in both endfire and sides directions according to the amount of phase delay introduced by the PSS. Length of the PSS controls power division between k_{-1} and odd-modes, and it can be changed utilizing active elements, for example, PIN diodes. Therefore, transmitted power level by the antenna can be intelligently controlled by altering ON/OFF diodes' states. The simulated and measured results are in good agreement, proving the validity of the method. The designed antennas are one-layer and very easy for fabrication with low cost and weight, making them useful for intelligent signal coverage in 5G and massive IoT communication systems.

ACKNOWLEDGMENT

The authors would like to keep names and memories of Prof. Pedram Mousavi and Prof. Mojgan Daneshmand alive for their exceptional support our research projects at the University of Alberta.

REFERENCES

[1] P. Mogensen and I. Rodriguez, "5G for smart production," in *The Future of Smart Production for SMEs: A Methodological and Practical Approach Towards Digitalization in SMEs*. Cham, Switzerland: Springer, 2022, pp. 327–333.

[2] G. Mei, N. Xu, J. Qin, B. Wang, and P. Qi, "A survey of Internet of Things (IoT) for geohazard prevention: Applications, technologies, and challenges," *IEEE Internet Things J.*, vol. 7, no. 5, pp. 4371–4386, May 2020.

[3] J. Pendry, L. Martin-Moreno, and F. Garcia-Vidal, "Mimicking surface plasmons with structured surfaces," *Science*, vol. 305, no. 5685, pp. 847–848, 2004.

[4] S. A. Maier, S. R. Andrews, L. Martin-Moreno, and F. Garcia-Vidal, "Terahertz surface plasmon-polariton propagation and focusing on periodically corrugated metal wires," *Phys. Rev. Lett.*, vol. 97, no. 17, 2006, Art. no. 176805.

[5] L. Jidi, X. Cao, J. Gao, S. Li, H. Yang, and T. Li, "Excitation of odd-mode spoof surface plasmon polaritons and its application on low-pass filters," *Appl. Phys. Exp.*, vol. 13, no. 8, 2020, Art. no. 84004.

[6] M. Du, Y. Feng, K. Chen, and J. Zhao, "Filtering microwave differential signals through odd-mode spoof surface plasmon polariton propagation," *J. Phys. D, Appl. Phys.*, vol. 53, no. 16, 2020, Art. no. 165105.

[7] S. Shen, B. Xue, M. Shi, and J. Xu, "Odd-mode and even-mode SSPPs transmissions based on complementary comb-like structure," *J. Electromagn. Waves Appl.*, vol. 33, no. 18, pp. 2499–2512, 2019.

[8] X. Gao, L. Zhou, and T. J. Cui, "Odd-mode surface plasmon polaritons supported by complementary plasmonic metamaterial," *Sci. Rep.*, vol. 5, no. 1, pp. 1–5, 2015.

[9] K. Zhuang et al., "Pattern reconfigurable antenna applying spoof surface plasmon polaritons for wide angle beam steering," *IEEE Access*, vol. 7, pp. 15444–15451, 2019.

[10] Q. Fu, H. Ni, G. Q. Luo, L. Zhu, and L. Liu, "A high aperture efficiency endfire antenna based on spoof surface plasmon polaritons," *IEEE Trans. Antennas Propag.*, vol. 71, no. 1, pp. 50–57, Jan. 2023.

[11] S. Li, Q. Zhang, Z. Xu, H. Zhao, and X. Yin, "Phase transforming based on asymmetric spoof surface plasmon polariton for endfire antenna with sum and difference beams," *IEEE Trans. Antennas Propag.*, vol. 68, no. 9, pp. 6602–6613, Sep. 2020.

[12] Y. Han et al., "Shared-aperture antennas based on even-and odd-mode spoof surface plasmon polaritons," *IEEE Trans. Antennas Propag.*, vol. 68, no. 4, pp. 3254–3258, Apr. 2020.

[13] X. Du, H. Li, and Y. Yin, "Wideband fish-bone antenna utilizing odd-mode spoof surface plasmon polaritons for endfire radiation," *IEEE Trans. Antennas Propag.*, vol. 67, no. 7, pp. 4848–4853, Jul. 2019.

[14] A. M. Patel and A. Grbic, "A printed leaky-wave antenna based on a sinusoidally-modulated reactance surface," *IEEE Trans. Antennas Propag.*, vol. 59, no. 6, pp. 2087–2096, Jun. 2011.

[15] A. Oliner and A. Hessel, "Guided waves on sinusoidally-modulated reactance surfaces," *IRE Trans. Antennas Propag.*, vol. 7, no. 5, pp. 201–208, Dec. 1959.

[16] M. Wang, J. R. Chen, Z. W. Cheng, H. F. Ma, and T. J. Cui, "High-efficiency leaky wave antenna based on periodic field-distribution modulation of single-conductor comb lines," *IEEE Trans. Antennas Propag.*, vol. 71, no. 12, pp. 9968–9973, Dec. 2023.

[17] Y. Jiang, L. Liu, Y. Hu, and D. Jiang, "Wideband small aperture endfire antenna based on spoof surface plasmon polaritons," *IEEE Trans. Antennas Propag.*, vol. 69, no. 8, pp. 5026–5031, Aug. 2021.

[18] L. Liu, Y. Jiang, Y. Hu, D. Jiang, and L. Zhu, "Wideband millimeter-wave endfire antenna based on symmetrical spoof surface plasmon polaritons," *IEEE Trans. Antennas Propag.*, vol. 69, no. 11, pp. 7386–7393, Nov. 2021.

[19] Y. Han et al., "Multibeam antennas based on spoof surface plasmon polaritons mode coupling," *IEEE Trans. Antennas Propag.*, vol. 65, no. 3, pp. 1187–1192, Mar. 2017.

[20] D. Tian, J. Wang, A. Kianinejad, A. Zhang, and Z. N. Chen, "Compact high-efficiency resonator antennas based on dispersion engineering of even-mode spoof surface plasmon polaritons," *IEEE Trans. Antennas Propag.*, vol. 68, no. 4, pp. 2557–2564, Apr. 2020.

[21] A. Kandwal et al., "Broadband frequency scanning spoof surface plasmon polariton design with highly confined endfire radiations," *Sci. Rep.*, vol. 10, no. 1, pp. 1–10, 2020.
[22] K. Zhang, D. Li, K. Chang, K. Zhang, and D. Li, *Electromagnetic Theory for Microwaves and Optoelectronics*. Heidelberg, Germany: Springer, 1998.
[23] G. S. Kong, H. F. Ma, B. G. Cai, and T. J. Cui, "Continuous leaky-wave scanning using periodically modulated spoof plasmonic waveguide," *Sci. Rep.*, vol. 6, no. 1, pp. 1–9, 2016.

BEHNAM MAZDOURI was born in Tehran, Iran, in 1992. He received the B.S. degree in electrical engineering from Semnan University, Semnan, Iran, in 2014, and the M.S. degree in electrical engineering from Shahed University, Tehran, in 2017. He is currently pursuing the Ph.D. degree with the Intelligent Wireless Technology Lab, The University of Alberta, Edmonton, Canada.

His research interests include the design and fabrication of intelligent THz and optical metasurfaces, passive and active microwave devices, antenna engineering, electromagnetic theories, and superconducting microwave devices, as well as the modeling of non-linearity in superconductive structures. He was a recipient of the Alberta Innovates Technology Futures Scholarship in 2021, and in 2022, he received the Mojgan Daneshmand and Pedram Mousavi Flight PS 752 Memorial Graduate Scholarship at The University of Alberta.

RASHID MIRZAVAND (Senior Member, IEEE) received the B.Sc. degree in electrical engineering from the Isfahan University of Technology, Isfahan, Iran, in 2004, and the M.Sc. and Ph.D. degrees in electrical engineering from the Amirkabir University of Technology (Tehran Polytechnic), Tehran, Iran, in 2007 and 2011, respectively.

He is currently an Assistant Professor with the Department of Electrical and Computer Engineering, The University of Alberta, Edmonton, AB, Canada, where he leads the Intelligent Wireless Technology Group. He is also an Adjunct Fellow with the Faculty of Engineering and IT, University of Technology Sydney, Australia. He has three granted and eight filled U.S. patents and is the coauthor of more than 100 journal and 70 conference papers. His major research interests include, but are not limited to, RF/microwave/mm-wave circuits, sensors, reconfigurable intelligent surfaces and antennas, numerical methods, and measurement systems.

Dr. Mirzavand received various awards, such as the Best AUT M.Sc. Researcher in 2007, the Best AUT Ph.D. Researcher in 2011, the Best MICT National Researcher in 2013, the National Elite Foundation Young Professor Grant in 2014, the AITF Elite PDF in 2015, the Honorable CMC Industrial Collaboration in 2017, the TEC Edmonton Innovation in 2019, the CMC Industrial Collaboration in 2021 as a Supervisor, the UofA Innovation in 2021, and three UofA Innovation in 2022. He is a Registered Member of the Association of Professional Engineers and Geoscientists of Alberta. He serves as a Specialty Chief Editor for *Frontiers in the Internet of Things* (IoT Enabling Technologies Section).